GAS ASSISTED CAVITY FORMATION AND BLISTERING IN CERAMICS —

S. J. Zinkle (Oak Ridge National Laboratory)

SUMMARY

Single- or poly-crystalline specimens of SiC, Si_3N_4, MgO, Al_2O_3 and $MgAl_2O_4$ were implanted with 0.4-1 MeV H^+ or 0.4-1 MeV He^+ ion beams at room temperature and 650°C (~0.1 and 0.4 T_M) up to fluences of ~$1x10^{22}/m^2$. This produced peak implanted gas and displacement damage levels as high as ~50 at. % and 21 displacements per atom (dpa). The specimens were subsequently examined optically, and in cross-section using transmission electron microscopy. Subsurface blistering occurred for specimens irradiated to H^+ or He^+ fluences greater than about $3x10^{21}/m^2$ (~15 at. % implanted gas concentration), and surface exfoliation occurred for fluences above ~$1x10^{22}/m^2$. Helium was more effective at inducing blistering and exfoliation than H on an atomic basis. The threshold blistering and exfoliation fluences for both ions decreased with increasing temperature. Both H^+ and He^+ were found to be very effective in inducing matrix cavity formation, due to their low solubility in these ceramics. Cavity formation was observed to initiate at the periphery of dislocation loops in several cases. The bubble formation and blistering behavior of the ceramics was similar to that observed for metals irradiated at comparable homologous temperatures.

Introduction

Due to their low atomic number, ceramics such as Al_2O_3 and SiC produce high concentrations of gaseous (H, He) transmutation products when exposed to high energy neutrons. Calculations suggest that the helium transmutation rate in Al_2O_3 and SiC exposed to 14 MeV neutrons is about 60-200 appm/dpa, whereas the corresponding transmutation rate in a fission reactor is only about 1-5 appm/dpa [1-3]. It has been recognized for many years that helium can enhance cavity formation in materials due to its limited solubility. Hydrogen has limited solubility in most ceramics and therefore might be more easily trapped in ceramics than in metals. In addition, hydrogen may react chemically with some ceramics [4]. The purpose of this report is to summarize some of the surface and bulk microstructural changes observed in H and He implanted MgO, Al_2O_3, $MgAl_2O_4$, Si_3N_4, and SiC, including the threshold fluences for blistering and exfoliation.

Experimental Procedure

Polycrystalline blocks of Al_2O_3 (GE Lucalox or Wesgo Al995), MgO (Ube UMP-0505), $MgAl_2O_4$ (Ceradyne) ß-SiC (Cercom) and Si_3N_4 (Kyocera SN733) and (0001)-oriented single crystal wafers of α-SiC (Cree) were machined into transmission electron microscope (TEM) samples using a combination of diamond sawing and ultrasonic cutting. The grain sizes of the polycrystalline specimens ranged from ~1 µm for the hot isostatically pressed Si_3N_4 to ~30 µm for the sintered oxide specimens. The polycrystalline samples were mechanically polished using 0.05 µm diamond paste, whereas the SiC single crystals were polished by the manufacturer. The specimens were bombarded in a 3x3 target array at room temperature or 650°C in the triple ion beam accelerator facility at Oak Ridge National Laboratory [5]. These temperatures correspond to ~0.15 and ~0.4 T_M for all of the materials except MgO, where T_M is the melting temperature (sublimation temperature for SiC and Si_3N_4). The irradiation temperatures corresponded to 0.1 and 0.3 T_M for MgO. The H and He irradiations were performed as part of a larger irradiation program on the effect of irradiation spectrum on dislocation loop formation and growth.

The specimens were exposed to H or He ion beams with energies ranging from 0.4 to 1 MeV. Typical particle fluxes for the irradiation ranged from 0.8-$6x10^{17}$ H/m^2-s and 0.4-$4x10^{17}$ He/m^2-s. Some specimens were also exposed to simultaneous dual beams of H and He ions with H/He flux ratios ranging from 3 to 10. The maximum fluences were $1.7x10^{22}$ H/m^2 and $1x10^{22}$ He/m^2, which correspond to calculated peak damage and implanted gas ion concentrations of 3 dpa and 60

at.% H and 21 dpa and 50 at.% He for 1 MeV H and 1 MeV He ions, respectively, assuming an average displacement energy of 40 eV. The implanted ion depths were ~10 μm and ~2 μm for 1 MeV H and 1 MeV He ions, respectively.

Following irradiation, the samples were examined with an optical microscope to detect blistering and surface exfoliation. Selected samples were prepared for cross-section TEM using techniques that are described elsewhere [6]. The TEM specimens were examined in a Philips CM-12 or CM-30 electron microscope, operating at 120 and 300 keV, respectively.

Results and Discussion

Threshold fluences for blistering and surface exfoliation

Figure 1 shows the low-magnification optical microstructures of several specimens following high-fluence H or He ion irradiation at 650°C. The dark regions correspond to surface exfoliation. Pronounced surface exfoliation occurred in the proton-irradiated oxide specimens after $1.7 \times 10^{22}/m^2$, with the largest percentage exfoliation occurring in $MgAl_2O_4$. Blistering was observed in proton-irradiated Si_3N_4 at $0.4\text{-}1 \times 10^{22}/m^2$, but surface exfoliation did not occur. Surface exfoliation occurred in all of the oxide specimens irradiated with 1 MeV He ions to $1 \times 10^{22}/m^2$, as well as in ß-SiC irradiated to $0.4 \times 10^{22}/m^2$.

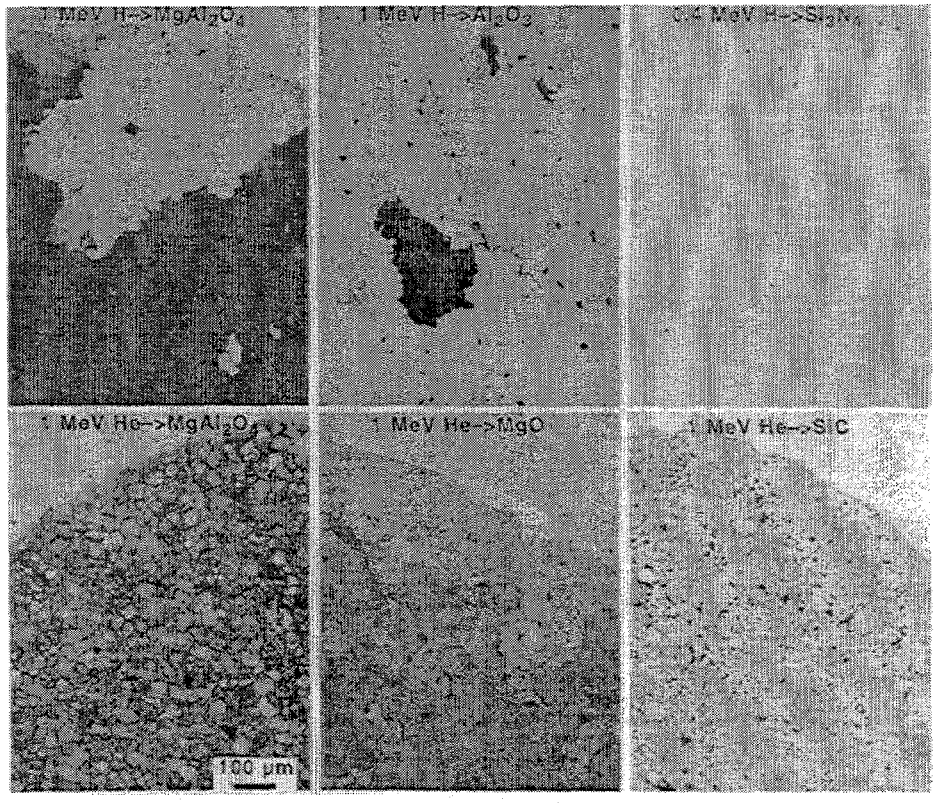

Fig. 1. Optical micrographs of polycrystalline Al_2O_3, MgO, $MgAl_2O_4$, Si_3N_4 and ß-SiC implanted at 650°C with 1 MeV H ($1.7 \times 10^{22}/m^2$), 0.4 MeV H ($1.0 \times 10^{22}/m^2$), or 1 MeV He ($1.0 \times 10^{22}/m^2$ for the oxides and $0.4 \times 10^{22}/m^2$ for SiC).

Optical examination of the irradiated samples indicated that blister formation and surface exfoliation generally occurred in specimens irradiated to fluences above ~$3x10^{21}/m^2$ and ~$1x10^{22}/m^2$, respectively. As discussed later in this section, blister formation was preceded by the formation of small cavities in the subsurface gas-implanted region. Hydrogen implantation generally required a higher fluence than the helium implantations to produce blistering or surface exfoliation. Table 1 summarizes the threshold H and He ion fluences for producing blistering and surface exfoliation at room temperature and 650°C. The threshold dose to produce blistering and surface exfoliation decreased with increasing temperature, in agreement with results previously obtained on metals [7]. Silicon nitride and single crystal SiC had the highest resistance to blistering and exfoliation, although most of the materials exhibited roughly comparable behavior. It is worth noting that the single crystal SiC specimens exhibited similar threshold doses for blistering and exfoliation, whereas the polycrystalline SiC and other ceramics typically blistered at doses two to three times lower than the dose required to produce surface exfoliation.

The present observations are in general agreement with previous extensive studies on metals [7,8] and limited data on ceramics [9-17] that the threshold fluence for blister formation occurs near 2 to $5x10^{21}/m^2$. The size of the blisters was noticeably smaller for He compared to H implantation, in agreement with previous studies on ceramics [10,11,13]. Surface exfoliation was generally limited to individual grains in the He-implanted specimens, whereas the blister formation and exfoliation extended over several grains in the H-implanted specimens (Fig. 1). These differences may be attributable to the deeper range of the H ions compared to the He ions (~10 vs. ~2 μm for 1 MeV ions in ceramics). Previous studies on metals have reported that the blister size increases with increasing implantation depth, with a roughly linear relationship of r/R~5 where r is the blister radius and R is the ion range [8].

Table 1. Summary of threshold fluences to produce blistering and surface exfoliation in H and He implanted ceramics. The parentheses denote conditions where blistering or exfoliation were not observed up to the maximum investigated fluence.

Ion and T_{irr}	Material	Blistering ϕt (10^{22} m^{-2})	Exfoliation ϕt (10^{22} m^{-2})
H, 50°C	α-SiC	(>1)	(>1)
"	Si_3N_4	(>0.3)	(>0.3)
"	Al_2O_3	~0.3	(>1)
"	$MgAl_2O_4$	~0.3	(>1)
H, 650°C	α-SiC	~0.8	~0.8
"	Si_3N_4	~0.4	(>1)
"	MgO	~0.3	~1
"	Al_2O_3	~0.3	~1
"	$MgAl_2O_4$	~0.2	~1
He, 50°C	α-SiC	(>0.5)	(>0.5)
"	Si_3N_4	~0.3	(>0.3)
"	Al_2O_3	~0.4	(>0.5)
"	$MgAl_2O_4$	~0.2	(>0.5)
He, 650°C	β-SiC	~0.2	~0.4
"	α-SiC	~0.8	~0.8
"	Si_3N_4	(>0.2)	(>0.2)
"	MgO	~0.3	~0.8
"	Al_2O_3	~0.3	~1
"	$MgAl_2O_4$	~0.1	~0.4

Although numerous studies have been performed on metals [18,19], relatively little is known about the microstructural effects of simultaneous high displacement damage and gas concentration in ceramics [16,20-25]. Therefore, cross-section transmission electron microscopy was performed on the H and He ion irradiated ceramic specimens to determine the physical processes responsible for the blistering and surface exfoliation. The cross-section technique allowed the microstructure of regions containing between zero and the maximum implanted gas concentration to be studied, in order to differentiate between displacement damage and implanted gas atom effects. Comparisons between specimens irradiated to different fluences provided a cross-check on the effect of implanted gas on the cavity evolution.

Effects of He on cavity formation

Helium implantation had a profound effect on cavity formation in $MgAl_2O_4$, where cavity formation is rare in the absence of gases [24,26-28]. The injected helium promoted cavity formation in the grain interior and at grain boundaries. Figure 2 compares the microstructures of $MgAl_2O_4$ irradiated with 1 MeV He ions at 650°C to fluences of 1×10^{21} and 1×10^{22} m^{-2}. The latter fluence corresponds to 21 dpa and 50 at. % He in the peak implanted region and ~2 dpa and ~0.08 at% He at a depth of 1.5 μm (0.5 μm from the peak implanted region). Small cavities (~2.5 nm average diameter) and a few extended microcracks were visible within a ~150 nm band (corresponding to the peak damage and injected He region) in the lower-dose specimen. Irradiation to an order of magnitude higher fluence produced only a slight increase in the average cavity diameter to ~5 nm within the peak implanted region, indicating that the cavity growth rate was slow (Fig. 2). Extensive cracking occurred within the He implanted region at the higher fluence.

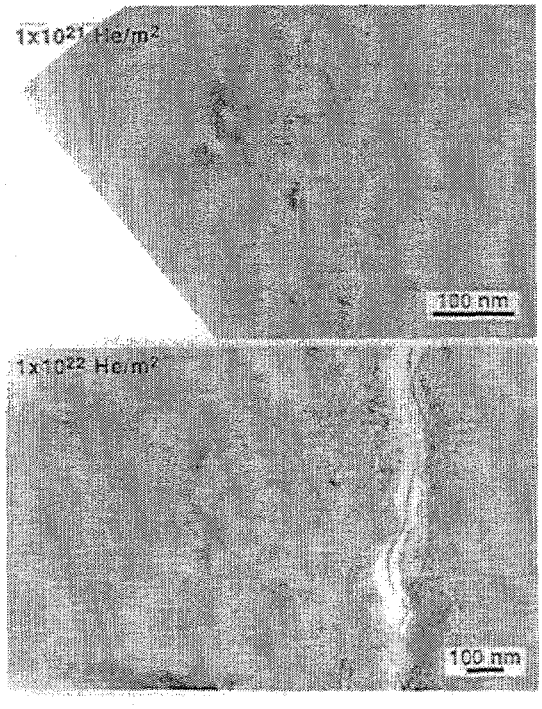

Fig. 2. Comparison of the cross-section microstructures of $MgAl_2O_4$ implanted with 1 MeV He ions at 650°C to fluences of 0.1 and 1×10^{22} m^{-2}.

Cavities were visible at all depths from the bombarded surface (0.5 dpa) to the implanted ion region (21 dpa) at the higher fluence. The cavity size was nearly constant in irradiated regions outside the peak implanted region (d=3.0 nm at the surface and d=3.3 nm at a depth of 1.5 μm) in the higher fluence spinel specimen. The corresponding cavity density increased from $4x10^{21}/m^3$ at the surface to $1.5x10^{22}/m^3$ at a depth of 1.5 μm.

A previous simultaneous dual-beam (He plus heavy ion) irradiation study on $MgAl_2O_4$ found that cavity formation was enhanced at dislocation loops and adjacent to grain boundaries [23]. At high dual-beam doses, the cavities completely envelop the grain boundary during irradiation at 650°C [23].

In agreement with previous ion irradiation studies on Al_2O_3 [20,21,23,29] and SiC [30,31] performed at temperatures above 500°C, the main effect of He implantation in α-SiC and Al_2O_3 was to enhance the formation of cavities along (0001) basal plane dislocation loops. Irradiation to high fluence ($\sim 1x10^{21}/m^2$) produced cracking in the helium-implanted region. The threshold dose for cavity formation was not determined in the present high-dose study, where cavity formation was observed in all specimens irradiated at 650°C (minimum investigated fluence of $1x10^{21}/m^2$). The results from previous studies suggest the threshold dose for cavity formation in He ion irradiated SiC and Al_2O_3 at 500-800°C is $\sim 1x10^{20}/m^2$ [20,24,31,32].

The threshold doses for cavity formation in SiC, Al_2O_3, $MgAl_2O_4$, and Si_3N_4 irradiated with He ions at room temperature were found to be ~1.0, 1.0, 1.0, and $1.5x10^{21}/m^2$, respectively. The formation of bubbles in He ion irradiated SiC was preceded by amorphization in the peak damage region. These observations agree with previous work on SiC [33] and Al_2O_3 [17] irradiated at room temperature. Chen et al. [25] observed He platelet formation on (0001) habit planes in α-SiC after room temperature implantation of 0.025 at. % He (0.15 dpa), where a degrader wheel was used to produce a uniform depth distribution of implanted He ($2.3x10^{22}/m^2$ total fluence). The lack of amorphization prior to bubble formation in the latter study may be attributable to a slightly higher irradiation temperature, since the amorphization dose for SiC is very sensitive to temperature near 300-350 K [34,35].

Effects of H on cavity formation

Hydrogen stimulates cavity formation in ceramics via impurity (gas pressure) effects, and may also exert chemical effects. However, higher hydrogen fluences were generally required to produce visible cavities compared to helium ion irradiation. The threshold fluence to produce visible cavities at 650°C ranged from $\sim 1 \times 10^{21}$ m^{-2} for $MgAl_2O_4$ to $\sim 1 \times 10^{22}$ m^{-2} for Si_3N_4, with the other ceramics lying at intermediate fluences. The threshold fluence to produce visible cavities at room temperature was ~5 to 10×10^{21} m^{-2} for $MgAl_2O_4$. Hojou et al. [33] found that formation of cavities in α-SiC at room temperature required a 15-keV H ion fluence of $\sim 5 \times 10^{22}$ m^{-2}, i.e., fifty times higher than the corresponding fluence for low energy He ion irradiation.

Figure 3 shows an example of small (~5 to 10 nm diameter) platelet cavities associated with (0001) dislocation loops in SiC implanted with 0.4 MeV H at 650°C. The original surface spalled off during the irradiation, so the fluence in the region shown in Fig. 3 is less than the specimen exposure fluence of 1×10^{22} H/m^2. The microstructure in the H-implanted region (gas-filled platelets) is similar to that observed in He-implanted SiC [25,30,31].

Figure 4 shows the microstructure of MgO after high-fluence implantation with 1 MeV H ions. Cavity formation in the implanted hydrogen region was preferentially associated with dislocation loops lying on {001} and {110} habit planes. Since hydrogen diffusion has been reported to be

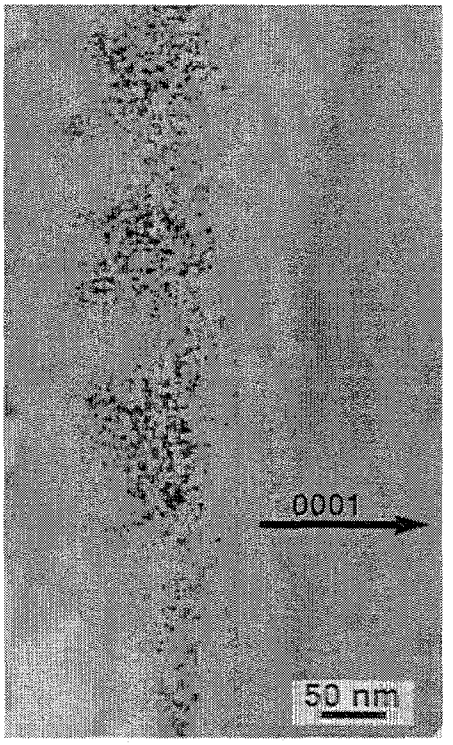

Fig. 3. Over focused cross-section microstructure of α-SiC implanted with 0.4 MeV H ions at 650°C. Due to surface exfoliation during the irradiation, the fluence in the displayed region is less than the specimen exposure fluence of 1×10^{22} H/m^2.

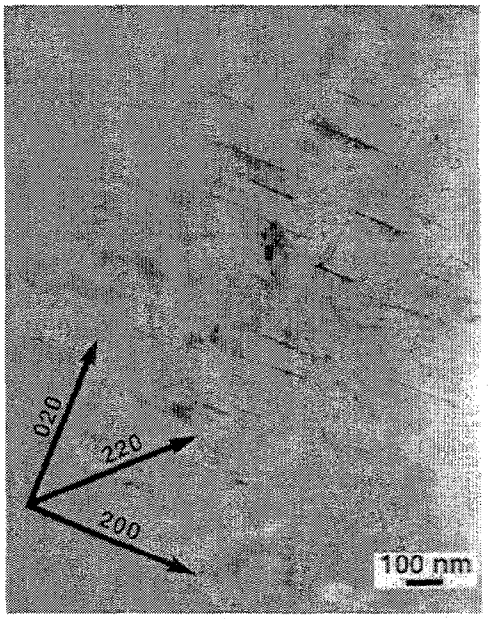

Fig. 4. Microstructure of MgO near the damage peak after irradiation with 1 MeV H ions at 650°C to a fluence of 1.7×10^{22} m^{-2}. The zone axis is near (001).

considerably enhanced by the ionizing radiation associated with proton irradiation [36], it is possible that much of the implanted hydrogen may have diffused away from the bombarded region during the irradiation.

Hydrogen implantation in Al_2O_3 at 650°C induced the formation of a high density of heterogeneously nucleated cavities. Figure 5 shows the cross-section microstructure of the peak damage region in Al_2O_3 following 1 MeV H ion irradiation at 650°C (3 dpa, 60 at.% implanted hydrogen at peak). The cavities were spatially segregated into regions containing high and low densities of cavities, with a mean cavity diameter of ~7 nm. The volume-averaged cavity density in the peak damage region was ~$6 \times 10^{22}/m^3$ and the mean diameter was ~5 nm. Examination of the irradiated regions adjacent to the peak damage region suggested that the heterogeneous grouping of individual cavities was due to their association with dislocation loops, as shown in Fig. 6. The two arrows in Fig. 6 point to dislocation loops which have 7 to 8 cavities associated with the periphery of the loops. The calculated damage level and implanted hydrogen concentration in this region are 0.3 dpa and 0.1 at.% H, respectively. Other loops depicted in Fig. 6 have cavities distributed along the entire face of the loop. Preferential nucleation of cavities at dislocation loops in H ion irradiated Al_2O_3 has been observed in another recent study [37].

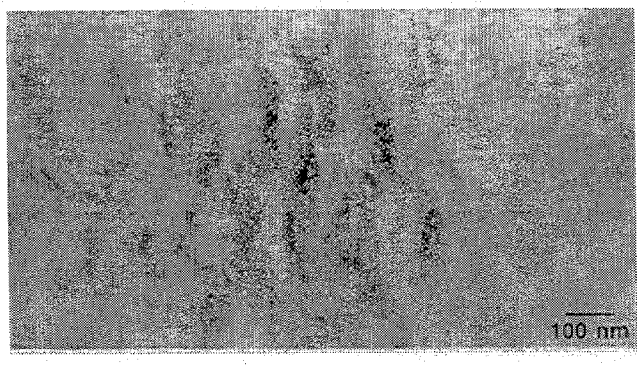

Fig. 5. Cavity formation in the peak damage region of Al_2O_3 irradiated with 1 MeV H ions at 650°C to a fluence of 1.7×10^{22} H/m^2.

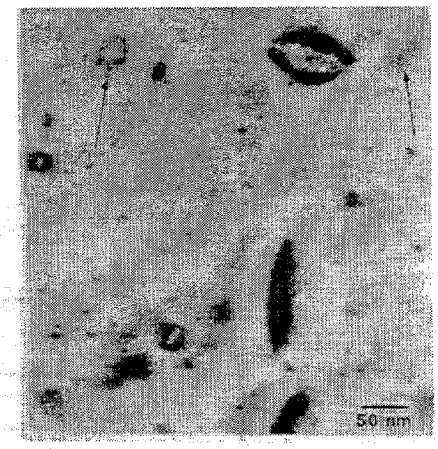

Fig. 6. Cavity formation at dislocation loops in Al_2O_3 irradiated with 1 MeV H ions at 650°C to 1.7×10^{22} H/m^2. The microstructure corresponds to an irradiation depth of ~9 μm (1 μm from the peak implanted region).

As shown in Fig. 7, irradiation of $MgAl_2O_4$ with 1 MeV H ions at 650°C produced a low to moderate density of cavities in the peak implanted region for a fluence of 1.5×10^{21} m^{-2} (0.28 dpa, 5.6 at. % H). The cavity density in the hydrogen-implanted regions of $MgAl_2O_4$ (~$1.5 \times 10^{21}/m^3$) was considerably lower and the cavity size (~10 nm) was higher than that in Al_2O_3 irradiated at comparable conditions. Irradiation of $MgAl_2O_4$ with 1 MeV H ions to an order of magnitude higher fluence produced matrix cavity growth and extensive cavitation along grain boundaries. The matrix cavities were faceted along {111} planes and were as large as 300 nm diameter. Figure 8 shows an example of the grain boundary cavities in $MgAl_2O_4$ irradiated with 1 MeV H ions to high fluence.

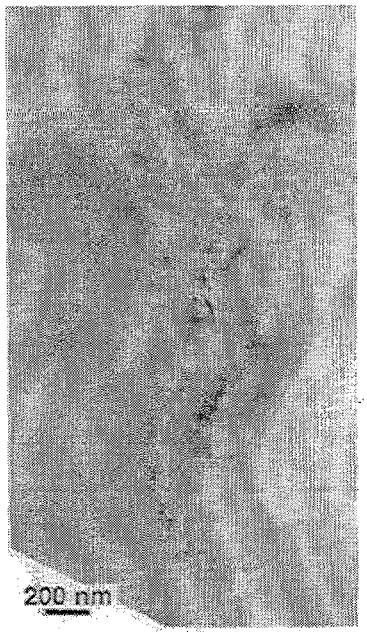

Fig. 7. Cross-section microstructure of $MgAl_2O_4$ irradiated with 1 MeV H ions at 650°C to a fluence of 1.5×10^{21} m^{-2} (0.28 dpa, 5.6 at.% H at peak).

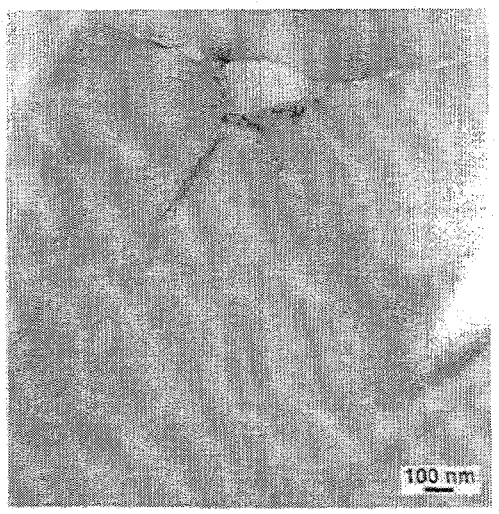

Fig. 8. Grain boundary cavities in $MgAl_2O_4$ irradiated with 1 MeV H ions at 650°C to a fluence of 1.7×10^{22} m^{-2}.

Figure 9 shows the low-magnification microstructure for $MgAl_2O_4$ irradiated with simultaneous beams of 0.4 MeV H and 0.36 MeV He ions at 650°C. In addition to the extensive matrix cavitation associated with the implanted H ions at a depth of ~2.7 μm, cavities were observed along the grain boundaries of the unirradiated region to depths in excess of 20 μm from the implanted region. The inset photo in Fig. 9 shows the grain boundary cavities observed at a depth of ~15 μm. It appears that the hydrogen had a chemical reaction with the non-spinel grain boundary phase present in the sintered polycrystalline $MgAl_2O_4$ specimen. Using a typical bulk diffusion coefficient for hydrogen in single crystal ceramics of $D_H \sim 1 \times 10^{-18}$ m^2/s at 650°C [38], hydrogen diffusion distances of only ~0.2 μm would be anticipated for the 8 h ion irradiation. Conversely, the apparent high grain boundary diffusivity suggested by Fig. 9 is consistent with effective diffusion coefficients of $D_H \sim 1 \times 10^{-14}$ m^2/s at 650°C measured for polycrystalline ceramics [38].

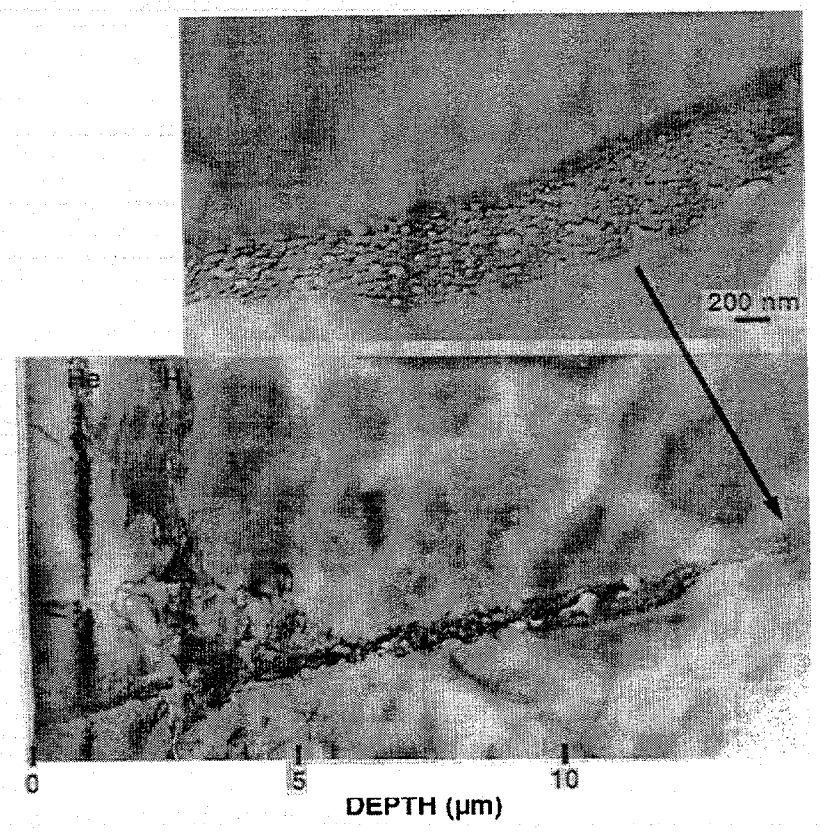

Fig. 9. Cross-section microstructure of $MgAl_2O_4$ irradiated at 650°C with simultaneous dual beams of 0.4 MeV H and 0.36 MeV He at a H/He flux ratio of 10 and a cumulative H fluence of 1×10^{22} m^{-2}.

Blistering mechanisms

The TEM observations indicate that blistering and surface exfoliation in H and He irradiated ceramics at 50 and 650°C is due to progressive cracking at the ligatures between highly pressurized gas bubbles that form in the implanted ion region. The blistering is not associated with coarsening of gas bubbles, as proposed in an early gas pressure model [10]. The present observations are consistent with the lateral compressive stress model [39], which predicts that blistering occurs when internal stresses at the implantation-produced cavities exceed the yield strength. The observations are also consistent with the pressurized gas platelet model proposed by Chen et al. [25].

Conclusions

In all of the H and He implanted specimens, blistering and surface exfoliation occurred at 650°C above a critical fluence of ~3 and ~10 × 10^{21} m^{-2}, respectively (~15 and ~40 at.% implanted gas concentration, respectively). The threshold fluence for blistering and surface exfoliation was generally lower for helium irradiation compared to hydrogen irradiation. The behavior of the ceramic specimens is similar to that of metals which have limited H and He solubility. The experimental observations are qualitatively consistent with the lateral compressive stress model for blistering.

Cavity formation was generally of higher density and more spatially uniform for He compared to H irradiation. The cavities were often associated with dislocation loops, particularly for H ion irradiation. In the case of proton-irradiated Al_2O_3 at 650°C, cavity nucleation appears to occur on dislocation loops created previously during the irradiation. For proton-irradiated SiC and MgO, there is insufficient evidence to determine whether the dislocation loop formation or cavity formation occurs first. Long range diffusion of hydrogen along grain boundaries was observed in $MgAl_2O_4$.

References

[1] L.H. Rovner, G.R. Hopkins, Nucl. Tech. 29 (1976) 274.
[2] G.P. Pells, J. Nucl. Mater. 155-157 (1988) 67.
[3] R.J. LaBauve, R. Livak, F.W. Clinard, Jr., Adv. Ceramic Mater. 3 (1988) 353.
[4] K. Hojou, S. Furuno, T. Soga, K. Izui, J. Nucl. Mater. 179-181 (1991) 411.
[5] M.B. Lewis, W.R. Allen, R.A. Buhl, N.H. Packan, S.W. Cook, L.K. Mansur, Nucl. Instr. Meth. B 43 (1989) 243.
[6] S.J. Zinkle, C.P. Haltom, L.C. Jenkins, C.K.H. DuBose, J. Electron Microsc. Tech. 19 (1991) 452.
[7] K.L. Wilson, Nuclear Fusion special issue (1984) 85.
[8] G.M. McCracken, Rep. Prog. Phys. 38 (1975) 241.
[9] W. Primak, J. Appl. Phys. 34 (1963) 3630.
[10] W. Primak, J. Luthra, J. Appl. Phys. 37 (1966) 2287.
[11] W. Primak, J. Appl. Phys. 48 (1977) 1556.
[12] W. Primak, J. Nucl. Mater. 74 (1978) 84.
[13] D.M. Gruen, B. Siskund, R.B. Wright, J. Chem. Phys. 65 (1976) 363.
[14] C.J. McHargue, G.C. Farlow, M.B. Lewis, J.M. Williams, Nucl. Instr. Meth. B 19/20 (1987) 809.
[15] L. Romana, G. Fuchs, G. Massouras, P. Thevenard, Radiat. Eff. Def. Solids 115 (1990) 139.
[16] E.L. Fleischer, M.G. Norton, Heterogeneous Chemistry Reviews 3 (1996) 171.
[17] S. Furuno et al., Nucl. Instr. Meth. B 127/128 (1997) 181.
[18] H. Schroeder, H. Ullmaier, J. Nucl. Mater. 179-181 (1991) 118.
[19] B.N. Singh, H. Trinkaus, J. Nucl. Mater. 186 (1992) 153.
[20] W.R. Allen, S.J. Zinkle, J. Nucl. Mater. 191-194 (1992) 625.
[21] W.E. Lee, M.L. Jenkins, G.P. Pells, Philos. Mag. A 51 (1985) 639.
[22] K. Hojou, S. Furuno, K.N. Kushita, N. Sasajima, K. Izui, Nucl. Instr. Meth. B 141 (1998) 148.
[23] S.J. Zinkle, S. Kojima, J. Nucl. Mater. 179-181 (1991) 395.
[24] R. Yamada, S.J. Zinkle, G.P. Pells, J. Nucl. Mater. 209 (1994) 191.
[25] J. Chen, P. Jung, H. Trinkaus, Phys. Rev. Lett. 82 (1999) 2709.
[26] F.W. Clinard, Jr., G.F. Hurley, L.W. Hobbs, J. Nucl. Mater. 108&109 (1982) 655.
[27] S.J. Zinkle, J. Nucl. Mater. 191-194 (1992) 645.
[28] C. Kinoshita, K. Fukumoto, K. Fukuda, F.A. Garner, G.W. Hollenberg, J. Nucl. Mater. 219 (1995) 143.
[29] M.D. Rechtin, Radiat. Eff. 42 (1979) 129.
[30] K. Hojou, K. Izui, J. Nucl. Mater. 160 (1988) 147.

[31] K. Nakata, S. Kasahara, S. Shimanuki, Y. Katano, H. Ohno, J. Kuniya, J. Nucl. Mater. 179-181 (1991) 403.
[32] Y. Katano, H. Ohno, H. Katsuta, J. Nucl. Mater. 155-157 (1988) 366.
[33] K. Hojou, S. Furuno, K.N. Kushita, H. Otsu, K. Izui, J. Nucl. Mater. 191-194 (1992) 583.
[34] S.J. Zinkle, L.L. Snead, Nucl. Instr. Meth. B 116 (1996) 92.
[35] L.L. Snead, S.J. Zinkle, W.S. Eatherly, D.K. Hensley, N.L. Vaughn, J.W. Jones, in: Microstructural Processes During Irradiation, eds. S.J. Zinkle et al., MRS Symposium Proceedings vol. 540 (Materials Research Society, Warrendale, PA, 1999) p. 165.
[36] Y. Chen, M.M. Abraham, H.T. Tohver, Phys. Rev. Lett. 37 (1976) 1757.
[37] S. Furuno, N. Sasajima, K. Hojou, K. Izui, H. Otsu, T. Matsui, J. Nucl. Mater. 258-263 (1998) 1817.
[38] J.D. Fowler, R.A. Causey, D. Chandra, T.S. Elleman, K. Verghese, in: Radiation Effects and Tritium Technology for Fusion Reactors, CONF-750989, eds. J.S. Watson, F.W. Wiffen, vol. II (USERDA, Gatlinburg, TN, 1975) p. 423.
[39] E.P. EerNisse, S.T. Picraux, J. Appl. Phys. 48 (1977) 9.